"Per aspera ad astra..."

Contents

CHAPTER 1

Introduction to the stars in high energy

Let your imagination soar. Whe sitting on the old rocker looking at the sky with couple of good old whiskey you can easily start thinking about the universe. There are myliards of different kinds of cosmic objects, but what you see in the night sky are predominantly stars. Indeed, almost all the shiny dots in the sky are stars, most of then being exceptionally bright and close - just a tiny speck of the galaxy's total population. You may be able to spot a handful of other galaxies that are bright enough to be seen by the naked eye, however, all the exotic objects that we are imagination remain elusive. They are too faint to be observed easily, because they are not only far, far away, but they also usually shine on different wavelengths, not visible by the human eye.

Think about the distances in the universe. One of the most accurate explanations is the one from: Adams (1979) *"Space," it says, "is big. Really big. You just won't believe how vastly, hugely, mindbogglingly big it is. I mean, you may think it's a long way down the road to the chemist's, but that's just peanuts to space..."*

Consider this, sometimes you want to study processes in these extreme, very faint objects, but they are too faint and too far out in the universe. You are looking for a "laboratory" with similar processes, but located much closer to the observer. The X-ray binary stars can be comsidered s this kind of laboratories.

There are, of course, many interesting phenomena which could be studied in X-ray binaries or in non-binary X-ray stars. Several of them are mentioned in the motivation section.

I am mentioning about several various space objects in this work, but the main effort is made to study the post-shock region in the Intermediate Polars (IPs).

1.1 Motivation

We can easily find many reasons why to study stars in the high energy bands. We can consider the direct and the most common scientific applications like observations of the supernovae, black holes and neutron stars in X-ray binaries. But for the education purposes I prefer several other, very nice examples closer to the topic of this work.

- **Relativistic jet phenomena**: like it was proposed by Mirabel (2002) that the universal mechanism should be at work in all the relativistic jet sources in the universe. Better understanding of sources including: microblazars, AGNs and gamma-ray burst will help to gain a more comprehensive understanding of these phenomena. Microblazars can play a role of "space laboratories", where interesting processes last on different timescales as is the case with AGNs or GRBs.

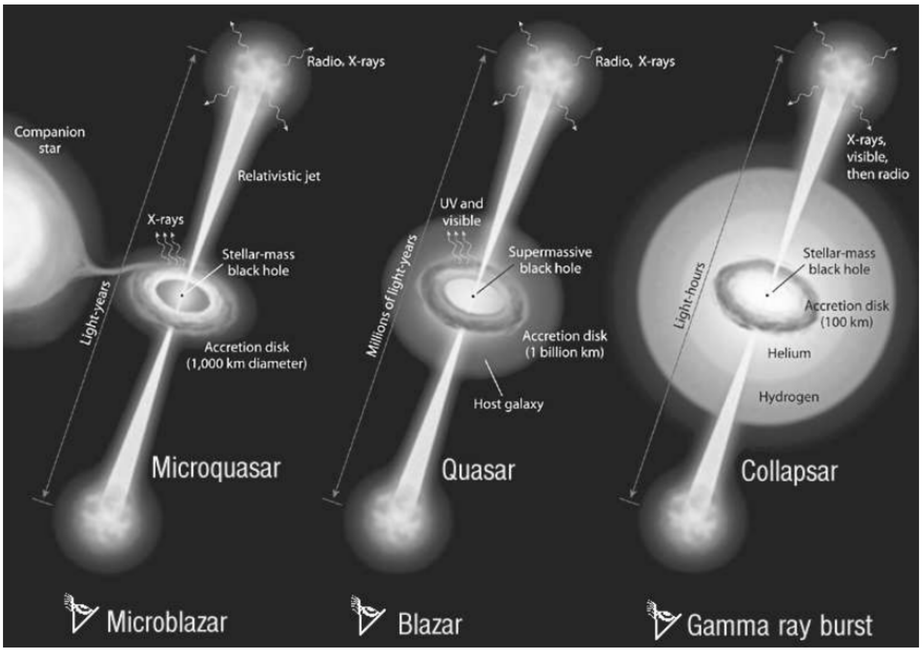

Figure 1.1: NOT in scale diagram, showing current ideas of micro-quasars, AGNs and gamma-ray bursts as space objects driven by the same, universal mechanism Mirabel (2002).

- **Galactic ridge X-ray emission (GRXE)**: various physical processes contribute to brightness of GRXE in different bands, but several studies in 3-20 keV provide evidence that the diffuse X-ray radiation originates from a huge number of stellar X-ray sources, mostly coronally active stars and white dwarf X-ray binaries. In particular for the energies over 20 keV to 200 keV, the spectrum is very similar to the spectrum of magnetic white dwarf binaries – e.g. Intermediate polars (IP) and polars (P). Krivonos et al. (2007)

- **White dwarfs' masses in Intermediate Polars (IP)**: as was proposed in Rothschild et al. (1981), the temperature of the post shock region (PSR) depends on WD mass. Therefor the X-ray spectrum can be used for WD mass determination Suleimanov et al. (2005). The WD mass estimations in cataclysmic stars is in general complicated. Usually, the curve of radiation velocities can be used, but it is quite hard to constuct. Therefore the X-ray spectrum method is very atractive for several reasons. This work is dedicated to this topic.

1.2 Aim of this work

To cover the whole topic: "stars in high energies" is far behind a capacity of a master thesis and because of that I have decided to concetrate on cataclysmic variable stars (CVs), especialy on intermediate polars (IPs).

As it will be mentioned in the next sections closely, IPs are magnetized CVs where the compact, primary star is a white dwarf with $B \sim 10^6 - 10^7$ Gauss. The mass accretion is taking place from, mainly a low-mass, non-degenerate star through its Roche lobe. The accretion disk is in some distance from the WD surface destroyed by a strong magnetic field and the accretion continues through, the so called, accretion curtain across the magnetic force-field.

The falling material in some point creates a stationary shock near the WD surface where the kinetic energy is converted through thermal bremsstrahlung to radiation. The temperature of the created plasma is typically more than 10 keV with a low density. The optically thin hard X-ray[1] emission is taking place and heated gas creates the post-shock region (PSR) with temperature gradient. The hot gas then descends and cools by the X-ray emission while it hits the WD surface.

Because of the relatively high temperature of PSR are IPs very well observed in hard X-rays band. IPs comprise only a small fraction $\sim 15\%$ of all CVs, but they dominate in hard X-ray band over 10keV, at most $\sim 80\%$ of detected CVs are IPs Landi et al. (2009).

The temperature of the PSR depends in first order only on the WD mass, which is the most fundamental parameter of WDs. This means, that if we are able to find temperature from fiting the thermal bremsstrahlung model to a spectrum of IP, we are also able to establish the WD's mass.

The accreting WDs are very important for cosmology, because some of such objects probably cause Type Ia supernovae, when the WD mass reaches Chandrasekhar limit.

As is showed on fig.(1.2), IPs as NY Lup are well observed by INTEGRAL/IBIS detector which makes them interesting space laboratories to investigate the basic

[1] In this case, hard X-rays means 10 - 120 keV region.

parameters of WDs. In same casesm, can by also accretion stream studied if it is strong enough.

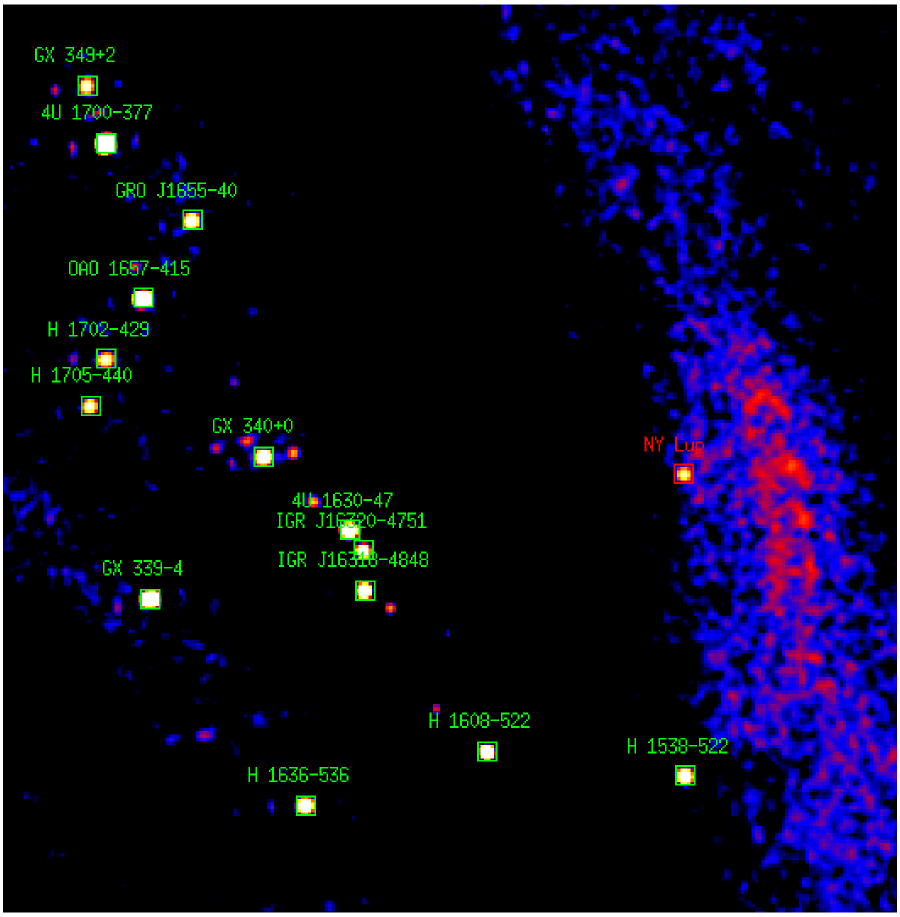

Figure 1.2: 1.2 Msec exposure of NY Lup region in 17-80 keV. The NY Lup is marked by red square. There are many others X-ray sources, mostly HMXBs or LMXBs.

1.3 Observations

Cataclysmic Variable stars (CVs) have been, in fact, observed as early as the ancient times. In the historical records of many civilizations we can find references for various astronomical events. Most of them are about objects that exhibits periodic variations of a some type, most notably: planets, Moon and Sun. However several of them are about comets and new stars. These new stars are in many cases novae and supernovae. In China, the records date back to 1500 BC.

Many records are saved from the medieval time, for example positions of Nova Vulpecula 1670 and Nova Cygni 1600 (now knows as P Cygni) in Hevelius maps.

With the advent of astronomical photography in the late 19th century started the era of continuous observations and with the development of first photo-multipliers in the mid-1940s CVs begun to be attractive targets because of their big variability in the different time scales.

The AAVSO has light curve of SS Cyg from 1896 up to date.

1.3.1 Optical and IR observations

The very first visual observation was followed by the photographic photometry and then spectroscopy, followed by the photo-multiplier photometry since mid-1940s. The binary nature of all CVs was confirmed. The flickering was discovered and was assumed that it is somehow connected to stars' duplicity Walker (1957), Warner (1995).

Statistical studies by Luyten and Hughes in mid-1960th showed, that novae remnants have $M_V \approx 4$ and dwarf novae at quisence have $M_V \approx 7.5$. They conclude that the hot primary star in CVs must be WD or hot subdwarf Warner (1995).

The most important contribution of optical astronomy to this work is the discovery of large and variable circular polarization in several CVs. This helped to identify magnetic CVs, which were later divided to two categories, polars and intermediate polars.

There are more important discoveries in optical and IR bands in CVs subject. In the case of interest the Warner (1995) is te recommended book.

1.3.2 X-ray observations

The very first CV detected in X-rays was EX Hya observed by Uhuru X-ray space mission. Uhuru worked in 2.0 – 6.0 keV and in spite of its poor sensitivity the well-known 4U catalogue was created Forman et al. (1978) from its observations.

The NASA's HEAO[2] program followed with three space missions. As the X-ray detectors technology evolved, the number of detected CVs growed linearly. EXOSAT provided long and uninterrupted data for many CVs during its operation from May 1983 until April 1986. Similar results were obtained from Soviet mission Kvant 1 and Japan's Ginga. The high hopes were invested into ROSAT which provided the all-sky survey in the 0.1 – 2.0 keV but the expected huge number of new CVs was not discovered.

The situation slightly changes with RXTE[3] which after several years on orbit provided good data for several articles about WD masses Suleimanov et al. (2005). The data from RXTE are used in the new articles even $\sim$ 15 years after its launch Butters et al. (2011).

Several others missions were launched in the last ten years period. Few of them carried several detectors where one was sensitive in X-rays, like SUZAKU/XIS and Swift/XRT. But for the X-ray astronomy the year of 1999 was the most important

[2] High Energy Astronomy Observatory, The HEAO 2 was also known as The Einstein Observatory

[3] Rossi X-ray Timing Explorer

so far. The two major big observatories were launched on the Earth's orbit. The Chandra X-ray Observatory flew onboard STS-93 space shuttle Columbia on July and the XMM-Newton was launched onboard ESA's Ariane 5 rocket.

That was the beginning of the X-ray astronomy's golden era. During the last decade the combination of Chandra and XMM provided enormous data archives which will be useful for astronomers in another decades.

Sadly, there is no big X-ray observatory planned for the next decade. One of the bigger space mission will be Japan's ASTRO-H with several X-ray and gamma ray detectors on-board to cover broad high energy bands. The future of big ESA & NASA space mission Athena (formerly: Constellation-X, XEUS, IXO) is questionable because of budget cuts in both space agencies.

Fortunately, there are several data archives with open acces for anybody interested. This is a big challenge mainly for young astronomers, who are not directly involved in any big space mission program but want to do science. In this case, they don't need any special hardware, even modern laptops are powerful enough.

1.3.3 Gamma ray observations

In last millennium several space mission observed few CVs in bands from tens of keV to TeV.[4] The biggest breakthrough came with ESA's INTEGRAL space mission which was able to observed many CVs with its exceptional sensitivity and large field of view. Mostly intermediate polars. Only $\sim 2\%$ of all CVs are actually magnetic ones, but these ones are only visible in gamma rays. INTEGRAL/IBIS was been used to determine white dwarf masses by Landi et al. (2009).

Two others space missions have on-board detectors similar to INTEGRAL/IBIS with their sensitivity and coverage: the NASA's Swift/BAT and Japan's Suzaku/XRT. Both are widely used to study white dwarf masses in IPs Brunschweiger et al. (2009), Yuasa et al. (2010).

[4] The most studied CV from this era is AE Aqr (Meintjes 1990; Bowden et al. 1991)

CHAPTER 2

White Dwarfs

White dwarfs born when normall mass stars die. WDs are degenerated, late type stars with typical mass $\sim 1M_{\odot}$. Their typical radius is about 5000 km and mean density around $10^6 g.cm^{-3}$ Shapiro & Teukolsky (2004). They no longer burn nuclear fuel and if they don't have any other mather influx e.g. by accretion from close star, they slowly cools as they radiate away residual thermal enegy.

WDs support themselves against gravity by the pressure of electron degenerate gas and theyr interior is in the local thermal equilibrium, except the thin atmosphere.

2.1 First look of white dwarfs interior

WDs are a class of the less compact objects among the possible endpoints of the stellar evolution. The mass of the star is the main factor determining whether the star ends up as a WD, neutron star or a black hole. The medium mass stars with masses $M \lesssim 4M_{\odot}$[1] in some point of late state of their evolution gently spreads mass forming planetary nebulae. The rest of the star become the white dwarf.

Let's use data from the table 2.1 and try to assume the pressure inside of WD. For very rough estimation, we can use equation of mechanic equilibrium to compare WD with the Sun:

$$\mathrm{d}P = -G\frac{M\rho\,\mathrm{d}r}{r^2} \tag{2.1}$$

The ratio between variables P, M, ρ and r in the Sun case and P', M', ρ', r' in the WD's case can be written as follows:

[1] Also $M \lesssim 8M_{\odot}$ can be find in some literature Padmanabhan (2001).

Table 2.1: Basic statisticks of the compact objects Shapiro & Teukolsky (2004)

Object	Mass[a] $[M]$	Radius[b] $[R]$	Mean Density $[r.cm^{-3}]$	Surface Potential $[GM/Rc^2]$
Sun	$M_\odot$	$R_\odot$	1	10^{-6}
White Dwarf	$\lesssim M_\odot$	$\sim 10^{-2}R_\odot$	$\lesssim 10^7$	$\sim 10^{-4}$
Neutron Star	$\sim 1-3M_\odot$	$\sim 10^{-5}R_\odot$	$\lesssim 10^{15}$	$\sim 10^{-1}$
Black Hole	Arbitrary	$2GM/c^2$	$\sim M/R^3$	~ 1

[a] $M_\odot = 1.989 \times 10^{33} g$

[b] $R_\odot = 6.9599 \times 10^{10} cm$

$$M' = M,$$
$$r' = 10^{-2} r,$$
$$\rho' = 10^6 \rho,$$

From easy calculation we get:

$$dP' = -G\frac{M'\rho' dr'}{r'^2} = -G\frac{M \cdot 10^6 \rho \cdot 10^{-2} dr}{r^2 (10^{-2})^2} = 10^8 dP \tag{2.2}$$

From such results is eminent that there is something wrong with the WDs interior in comparation with central reion of the normal star. As the ionization is increasing by higher temperatures, the bigger pressure otherwise helps recombination. However very big pressure actually increase ionization up to totally ionized atoms. Atoms without their electrons shells are closer to each others which explains very high density.

For densities in range $10^5 gm.cm^{-3} \lesssim \rho \lesssim 10^9 gm.cm^{-3}$ the WD is made of ideal nondegenerate gas of ions and a degenerate gas of electrons. The system will be degenerate if $T > T_c$ where $T_c \approx 3 \times 10^9 K(\rho/\rho_c)^{2/3}$

If the electrons are relativistic or not can be found by comparing $m_e c$ with a fermi momentum

$$p_F = (3\pi^2)^{1/3} \hbar n_e^{1/3} = (3\pi^2)^{1/3} \hbar (\rho/\mu_e)^{1/3} \tag{2.3}$$

where

$$\mu_e = (\rho/n_e m_p) = 2(1+X)^{-1} \tag{2.4}$$

is the mass per electron. The fermi momentum will be equal to $m_e c$ at the critical density:

$$\rho_c \equiv \frac{8\pi}{3} m + p\mu_e \frac{m_e c^3}{h} \approx 10^6 \mu_e . gm.cm^{-3} \tag{2.5}$$

If the density is higher than $\rho \gtrsim 10^9 gm.cm^{-3}$, the electrons are combined with protons inside of nuclei and create different matter called neutron degenerated gas. This is how neutron stars are made.

2.2 Fermi energy

Now we can imagine interior of WDs as an area full of atoms nuclei very close to each other with free electrons around them. But electrons are fermions, which means that they must behave according to Pauli exclusion principle and it allows only at most one fermion per each quantum state.

If we imagine a normal, everyday gas at standard temperature and pressure, only one of every 10^7 quantum states is occupied by gas particles, so Pauli exclusion principle limitation is very insignificant. When energy is removed from the gas and it's temperature falls down, an increasingly large fraction of the particles been forced into the lower energy states.

For fermions gas only one particle can take the lowest energy state and others must take another, higher and higher states, thus only one particle per state is allowed. Even in limit $T \to 0$ pressure is produced by motions of electrons on excited positions.

At the zero temperature all of the lowest states and none of the higher states are occupied, this kind of fermion gas is called completely degenerated. The max energy of electron in completely degenerate gas at $T = 0K$ is known as Fermi energy.

For determining the limiting energy we can imagine 3D box where length of each of its sides will be L. The wavelengths of electrons trapped in the box in each dimension will be

$$\lambda_{xyz} = \frac{2L}{N_{xyz}} \tag{2.6}$$

where N_{xyz} are integer quantum numbers for each dimension. The momentum can be written through de Broglie wavelength

$$p_{xyz} = \frac{hN_{xyz}}{2L} \tag{2.7}$$

We can now write the total kinetic energy of the electron when $p^2 = p_x^2 + p_y^2 + p_z^2$ as follows

$$\varepsilon = \frac{p^2}{2m} \Rightarrow \frac{h^2N^2}{8mL^2} \tag{2.8}$$

Total number of electrons is same as total number of unique quantum numbers N_x, N_y, N_z, multiply by factor two. The two factor comes from the fact that electrons are particles with spin, which can be $\pm 1/2$. This means that two electrons are allowed to have the same tree quantum numbers but different spin. The total number of electrons out to radius $N = \sqrt{N_x^2 + N_y^2 + N_z^2}$ will be

$$N_e = 2\left(\frac{1}{8}\right)\left(\frac{4}{3}\pi N^3\right) \Rightarrow N = \left(\frac{3N_e}{\pi}\right)^{1/3}. \tag{2.9}$$

By using Eq. (2.8) and simplifying it, we will get the Fermi energy as follows

$$\varepsilon_F = \frac{\hbar^2}{2m}\left(3\pi^2 n\right)^{2/3} \tag{2.10}$$

where m is the mas of the electron or any other fermion[2] and $n \equiv N_e/L^3$ is the electron count per volume. The average energy per electron at $T = 0K$ is $\frac{3}{5}\varepsilon_F$.

2.3 Degeneracy

Matter inside of WD has very symmetric spherical distribution, we can calculate the mass interior to radius r like[3]

$$\frac{dm_{(r)}}{dr} = 4\pi r^2 \rho \tag{2.11}$$

In normal case the WD is in steady state and gravitation force is balanced by the pressure at every point. For deriving the hydrostatic equilibrium equation we need to consider an infinitesimal element laying between r and $r + dr$ with an area dA. The element is lying perpendicular to the radial direction, should looks like fig.(2.1).

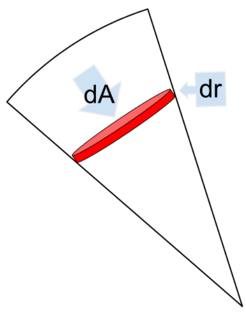

Figure 2.1: How could be infinitesimal fluid element laying between r and $r + dr$ with an area dA imagine

The gravitation attraction between mass $dm = \rho dAdr$ and $m_{(r)}$ is the same as if $m_{(r)}$ were only point at the center with the same mass. While the outside mass exerts no force on dm. Then the net outward pressure forced on dm is $-[P(r+dr) - p(r)]\,dA$. In equilibrium

$$\frac{dP}{dr} = -\frac{Gm_{(r)}\rho}{r^2} \tag{2.12}$$

In such equilibrium, the gradient of degeneracy pressure is balanced by gravitation:

$$\nabla P = -\rho \nabla \Phi, \tag{2.13}$$

[2]Can by applies for any fermion, not only electrons

[3]More elaborate and precises approach can by find Shapiro & Teukolsky (2004), Padmanabhan (2001), Kleczek (1957), Camenzind (2007), Nauenberg (1972) and simpler explanation with less math in Carroll & Ostlie (2007)

where Φ means gravitation potential. Consequence of the Eq.(2.12) is the viral theorem. The gravitation potential energy of the star is then

$$W = -\int_0^R \frac{Gm_{(r)}}{r}\rho 4\pi r^2 dr = \int_0^R \frac{dP}{dr} 4\pi r^3 dr = -3\int_0^R P 4\pi r^2 dr \tag{2.14}$$

We can characterize the gas by an adiabatic equation of state, where K and Γ are constants

$$P = K\rho_0^{\Gamma} \tag{2.15}$$

Then Eq.(2.14) can be rewritten as follows

$$W = -3(\Gamma - 1)U, \tag{2.16}$$

Where U is the total star's internal energy

$$U = \int_0^R \varepsilon' 4\pi r^2 dr \tag{2.17}$$

and ε' comes from:

$$\varepsilon' \equiv \varepsilon - \rho_0 c^2 \tag{2.18}$$

where

$$\varepsilon = \rho_0 c^2 + \frac{P}{\Gamma - 1} \tag{2.19}$$

Now we can see that the energy density, of the gas (excluding the rest mass energy) can be also written as

$$\varepsilon' = \frac{P}{\Gamma - 1} \tag{2.20}$$

Assuming adiabatic changes, the Eq.(2.20) follows from the first law of thermodynamics

$$d\left(\frac{\varepsilon}{\rho_0}\right) = -Pd\left(\frac{1}{\rho_0}\right). \tag{2.21}$$

The equation of state for ideal Fermi gas reduce to the simple polytropic form Eq.(2.15) in the two limiting cases Shapiro & Teukolsky (2004), Padmanabhan (2001):

- Nonrelativistic electrons, $\rho_0 \ll 10^6 g.cm^{-3}, x \ll 1, \Phi_{(x)} \to x^5/15\pi^5$

$$\Gamma = \frac{5}{3} \Longrightarrow K = \frac{3^{\frac{2}{3}}\pi^{\frac{4}{3}}}{5}\frac{\hbar^2}{m_e m_u^{\frac{5}{3}} u_e^{\frac{5}{3}}} = \frac{1.0036\times 10^{13}}{u_e^{\frac{5}{3}}} cgs. \tag{2.22}$$

- Extremly relativistic electrons, $\rho_0 \gg 10^6 g.cm^{-3}, x \gg 1, \Phi_{(x)} \to x^4/12\pi^2$

$$\Gamma = \frac{4}{3} \Longrightarrow K = \frac{3^{\frac{1}{3}}\pi^{\frac{2}{3}}}{4}\frac{\hbar c}{m_u^{\frac{4}{3}} u_e^{\frac{4}{3}}} = \frac{1.2435\times 10^{15}}{u_e^{\frac{4}{3}}} cgs. \tag{2.23}$$

This kind of the equilibrium configurations such these are called polytropes. We can use Eq.(2.13), take the divergence of it and by using $\nabla^2\Phi = 4\pi G\rho$ in spehrically symmetric case we get

$$\frac{1}{r^2}\frac{d}{dr}\left(\frac{r^2}{\rho}\frac{dP}{dr}\right) = -4\pi G\rho. \tag{2.24}$$

Using few trics, Eq.(2.24) can be rewrite and reduce to dimension less form

$$\frac{1}{\xi^2}\frac{d}{d\xi}\xi^2\frac{d\theta}{d\xi} = -\theta^n \tag{2.25}$$

use Eq.(2.15) with $\Gamma \equiv 1+\frac{1}{n}$ where n is called the polytropic index

$$\rho = \rho_c\theta^n \tag{2.26}$$

$$r = a\xi \tag{2.27}$$

$$a = \left[\frac{(n+1)\,K\rho_c^{(1/n-1)}}{4\pi G}\right]^{1/2} \tag{2.28}$$

where ρ_c is the central density, $\rho_c = \rho$ when $r = 0$.

The Eq.(2.25) is called the *Lane-Emden equation* for the structure of n index, the boundary conditions at the center such polytropic white dwarf are

$$\theta(0) = 1, \tag{2.29}$$

$$\theta'(0) = 0. \tag{2.30}$$

The condition (2.29) come dirrectly from Eq.(2.26) and condition (2.30) is derived from the fact that near the center of the star is $m_{(r)} \approx 4\pi\rho_c\frac{r^3}{3}$. If we use Eq.(2.12), we get

$$\frac{dP_{(\rho)}}{dr} = \frac{d\rho}{dr} = 0. \tag{2.31}$$

If we numerically integrate Eq.(2.25) using Eq.(2.29) and Eq. (2.30) as the boundary conditions, starting at $\xi = 0$. We will find that for $n < 5$ $(Gamma > \frac{6}{5})$ this solution decrease monotonically with a zero at finite value $\theta(\xi_1) = 0$, which corresponds to the star's surface where $P = \rho = 0$ and we get the equation for white dwarf radius

$$R = a\xi_1 = \left[\frac{(n+1)K}{4\pi G}\right]^{1/2}\rho_c^{\frac{1-n}{2n}}\xi_1. \tag{2.32}$$

The mass o thef WD can be find as follows

$$\begin{aligned} M &= \int_0^R 4\pi r^2 \rho dr \\ &= 4\pi a^3 \rho_c \int_0^{\xi_1} \xi^2 \theta^n d\xi \\ &= -4\pi a^3 \rho_c \int_0^{\xi_1} \frac{d}{d\xi}\left(\xi^2 \frac{d\theta}{d\xi}\right) d\xi \\ &= 4\pi a^3 \rho_c \xi_1^2 |\theta'(\xi_1)| \\ &= 4\pi \left[\frac{(n+1)K}{4\pi G}\right]^{3/2} \rho_c^{\frac{(3-n)}{2\pi}} \xi_1^2 |\theta'(\xi_1)|, \end{aligned} \tag{2.33}$$

then ρ_c can by eliminated between Eq.(2.32) and Eq.(2.33), which gives the mass-radius relations for polytropes Shapiro & Teukolsky (2004):

$$M = 4\pi R^{\frac{3-n}{t-n}} \left[\frac{(n+1)K}{4\pi G}\right]^{\frac{n}{n-1}} \xi_1^{\frac{3-n}{1-n}} \xi_1^2 |\theta'(\xi_1)| \tag{2.34}$$

2.4 The Chandrasekhar limit

What will happen if $\rho_c \rightarrow \infty$? This is one of the most important questions in the universe. Because how central density of WD increases by increase of the WD mass, the electrons become more and more relativistic throughout the star. As $R \rightarrow 0$ also the space for free electrons moving between atoms nuclei become smaller and smaller. With increasing mass must also increase the speed of electrons to support the degeneracy pressure. While the mass of WD is larger the radius become smaller, mass-volume relations implies that $\rho \propto M_{WD}^2$. But the electrons can't have speed larger than speed of light and in some point where $\rho \sim 10^9 gcm^{-3}$ there will be no space left for moving electrons and they will be press into the nuclei. This will leads to explosion of such WD.

This all means, that there is a maximum mass for WDs. This mass is called *Chandrasekhar limit* [4] M_{ch}.

The classical theory of type 1A supernovae assumes explosions of such WDs reaching the M_{ch}, the very same mass of the WDs when they explode makes Type 1A supernovae perfectly suitable objects for measuring the long range space distances. That's why they are so important objects for cosmology and astronomers called them standard candles.

The Chandrasekhar limit for relativistic electron case is

$$M = 1.457 \left(\frac{2}{\mu_e}\right)^2 M_{\odot}, \tag{2.35}$$

[4] Named after Indian physicist Subrahmanyan Chandrasekhar who received the Nobel Price in Physics in 1983 for his work on stellar structure and evolution. Chandrasekhar made his great discovery at the age of 21 in the 1931.

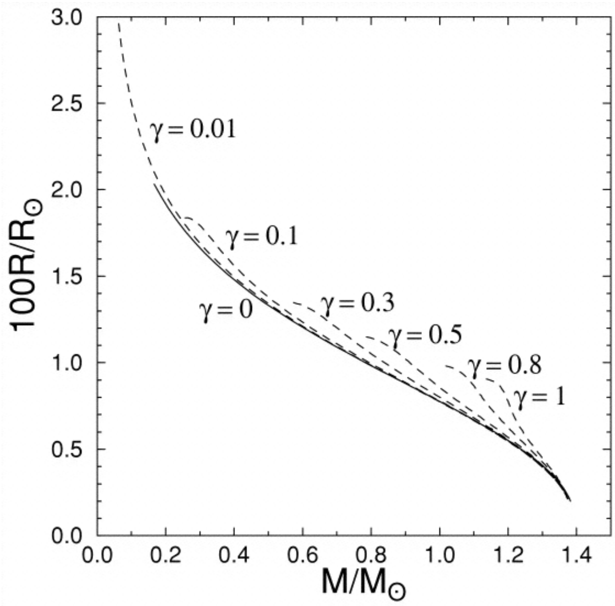

Figure 2.2: Relation between the mass M and radius R of a ^{12}C magnetic white dwarf for the indicated magnetic field strengths. The solid line denotes the Hamada & Salpeter (1961) model for nonmagnetic white dwarfs $(\gamma = 0)$. The dashed lines are magnetic white dwarfs. Suh & Mathews (2000)

where μ_e is the average molecular weight per electron, which depends on the chemical comsposition of the star and is typically sets to $\mu_e = 2$.

The Eq.(2.35) can be obtained by solving Eq.(2.34) with parameters[5]:

$$\Gamma = \frac{4}{3}, n = 3, \xi_1 = 6.89685, \xi_1^2|\theta'(\xi_1)| = 2.01824. \tag{2.36}$$

Another, ilustrativ aproach to estimating the Chandrasekhar limit is mention in Carroll & Ostlie (2007). An approximate value for M_{ch} may by obtain by setting the estimate of the central pressure

$$P_c \approx \frac{2}{3}\pi G \rho^2 R_{wd}^2 \qquad \text{with} \qquad \rho = M_{wd} / \frac{4}{3}\pi R_{wd}^3 \tag{2.37}$$

equal to electron degeneracy pressure equation

$$P = \frac{(3\pi^2)^{2/3}}{4}\hbar c \left[\left(\frac{Z}{A} \right) \frac{\rho}{m_H} \right]^{4/3}, \tag{2.38}$$

with $\frac{Z}{A} = 0.5$, the R cancels from the equation leving for the greatest possible mass:

$$M_{ch} \sim \frac{3\sqrt{2\pi}}{8} \left(\frac{\hbar c}{G} \right)^{3/2} \left[\left(\frac{Z}{A} \right) \frac{1}{m_H} \right]^2 M_{\odot}. \tag{2.39}$$

[5]Extensive list of polytropic parameters can be find in Chandrasekhar (1939)

It is important to notice that Eq.(2.39) contains three fundamental constants $\hbar, c$ and G representing the combined effects of quantum mechanics, relativity and Newtonian gravitation on the WD structure.

The Chandrasekhar limit slightly depends upon the chemical composition (2.35), but in the literature is well known as $M_{ch} = 1.44 M_{\odot}$.

The similar limit exists for neutron stars, where pressure of degenerate neutron gas support the stars against it own gravity. This limit is called Tolman - Oppenheimer - Volkoff limit (or TOV limit).But it is not so easy in neutron stars case. Their limit mass depends strongly on type of matter in star center. The limit varies from $0.7M_{\odot}$ up to $\sim 3M_{\odot}$ in extreme case, when inner section of neutron star is partialy filled up by quark - gluon meatter.

2.5 White dwarfs classes

Previous sections describe interior and fundamental parameters of white dwarfs, but it also important to tell something about their classes. WDs occupy narrow sliver line in the left bottom corner of H-R diagram fig.(2.3), slightly parallel with the main sequence. Although WDs are typically whiter then normal stars, the name itself is not very comprehensive. WD in fact come in all colors with surface temperatures from less than $4000K$ to even more than $80,000K$. The *D* for *dwarf* spectral type has several subdivisions:

- **DA** white dwarfs is the largest group ($\sim 60\%$) including Sirius B, their spectra have only pressure-broadened hydrogen lines
- **DB** white dwarfs ($\sim 8\%$) have only helium absorbtion lines in their spectra
- **DC** white dwarfs ($\sim 14\%$) have no lines, but only continuum features
- **DQ** white dwarfs show carbon features in their spectra
- **DZ** white dwarfs show some evidence of metal lines

Very small radius makes WDs hard to observed in optical band. The brightest and also the most known WD is Sirius B with visual magnitude ~ 8.6. Unfortunately it is located only 8" from his companion Sirius A, the brightness star of the night sky. Although the WD are not common stars on the night sky, their are not rare in our Galaxy. From hundred closes stars to our Sun, eight of them are WDs.

WDs usually have very strong magnetic field which comes from weak surface magnetic field of progenitor's star which lagre surface are conserved to their very small surfaces. The magnetic field intensities vary from about $1000 gauss$ up to $10^9 gauss$ in extreme cases.

WDs can by find alone in interstellar space, young ones can be find also in planetary nebulae, like one in center of the Ring nebula M57 or their can be find in cataclysmic variables.

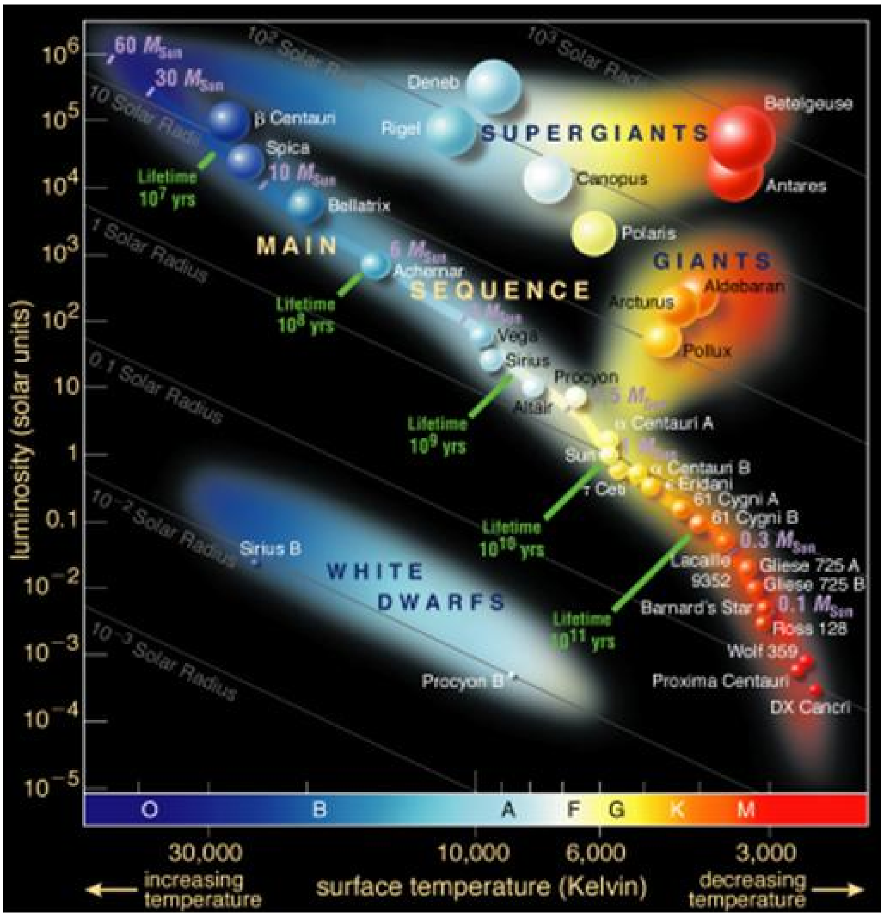

Figure 2.3: WD lies in right bottom corner of HD diagram, under main sequence, which exactly means, they are very small (dwarf) stars with high surface temperature.

CHAPTER 3

Cataclysmic variable stars

Cataclysmic variable stars *(CVs)* received their name for their cataclysmic events, like outbursts, novae and supernovae eruptions. In this one name several very different mechanisms are used for creating the various cataclysmic events. Dwarf novae are common for their increase of brightness by factor 10, classical novae are increasing their brightness usually in factor 10^6 and type 1A supernovae in factor 10^{12}, typical visual absolute magnitude for them is $M_v = -19.3$[1].

What is common for all the CVs types is their binary star character with mass transfer through Roche lobe to primary companion, which is white dwarf star. Several thousands of CVs with even more candidates are known up to date. The mean mass of the primary star is $\sim 0.8M_\odot$, which is larger than the average of $\sim 0.6M_\odot$ for isolated, forever alone WDs. The secondary star is a main-sequence low mass star of G or later type, but usualy with less mass then the primary WD.

Configuration like this make stars orbit each other with periods from around 20 minutes up to several days, however the vast majority of CVs have orbital periods from 1 to 12 hours[2].

The various classifications and approaches to study the CVs exists. They mostly depends on the different wavelength in which the CVs are observed. The biggest and also the well observed is optical band where we can see these types:

- **Classical novae** are characterize by large outbursts couses by thermonucler exlosion of acreated material on WD's surface
- **Recurrent novae** have small outbursts repeating every few 10 years, typical example is *RS Oph*

[1] About 5×10^9 times brighter than the Sun

[2] Interesting think is that there exists a "period gap" in CVs periods in range from 1.5 to 3.25 hours. The cause of this gap is not well understood yet.

- **DN - dwarf novae** use to have several smaller outbursts, have several sub-clases *(Z Cam, SU UMa, SS Cyg*[3]*)*
- **AM Canum Venaticorum** are extremely interesting space objects where the secondary star is also a compact object and the accretion disk is mostly composed from helium and they could by source of strong gravitation waves
- **Novae like systems** are possible nova remnants or stars with outburst behavior similar to novae but maybe miss-classify
- **Polars** are magnetic CVs with $B \sim 10^7 - 10^9 Gauss$, they got the name because of strong polarization of their light in optical and IR bands
- **IP intermediate polars** are magnetic CVs with B less then polars $\sim 10^6 - 10^7 Gauss$
- **Type 1A supernova** is sub-class of supernovae which become a result of thermonuclear explosion of whole WD when it reaches the M_{ch} limit

During last years CVs became more and more attractive target for modern astronomers mainly because of the progress in detectors technology in different then optical band and also for their role as a space laboratories for study accretion of matter on compact star, X-ray emission from shock regions, and even gravitation waves.

The CVs are complex and complicated space objects, for this reason is hard to make a good classification. If we look inside Warner (1995), we will find several fact which are not consider as correct now. With new huge sky surveys as GAIA[4] or LSST[5] the new and even more complex classification will need to take place. The number of known CVs systems will grow rapidly, also as the number of observations. Next decade will be the gold era for new scientific approaches like data-mining in huge amount of data-sets.

In following sections of this work we use the most broad CVs classification, for magnetic and non-magnetic systems. Because of the aim of this work on magnetic systems, we will take care of non-magnetic only roughly. Please also note, that if we want to make a very good classification of CVs to many classes, almost everyone of them will has its own class.

[3]SS Cygni had few outbursts, but according to latest obervations, it seems to be more-likely intermediate polar

[4]Is space mission to chart a three-dimensional map of our Galaxy, will observed $\sim$ one billion stars. Launch is planned for 2013.

[5]The Large Synoptic Survey Telescope (LSST) will be wide-field survey $8.4m$ telescope which will photograph the available sky every three nights from his place on the El Peñón peak of Cerro Pachón, at 2682 m in Chile.

3.1 Non magnetic cataclysmic variables

The magnetic field plays essential role in all the CVs, even in non-magnetic ones, at-least weak magnetic field provides viscosity in accretion disk. We will called non-magnetic CVs when $B \lesssim 10^5 Gauss$. In such system is movement of gas from the secondary companion to the WD determined predominantly by dynamical and hydro-dynamical flows Warner (1995).

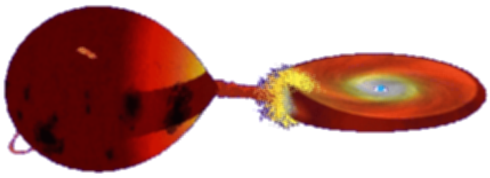

Figure 3.1: The illustration of cataclysmic variable star, showing the normal, secondary star on the right, accretion stream meeting the accretion disk and accretion disk itself around the white dwarf.

The non-magnetic CV could looks like fig.3.1 or the *(A)* part of fig.3.3. The secondary is a small main sequence star with mass about half of the Sun mass which is filling out its Roche lobe. The mass transfers from secondary to primary through the Lagrangian point L1 and in some point its creates the accretion disk. Streaming mass meets the accretion disk and if the mass stream is big enough and disk is dense enough, so called hot spot is created as we can see on fig.3.1.

3.1.1 Orbital periods

Orbital period P_{orb} is usually the most precisely know physical parameter of CV. Because of facts that the CVs orbital periods are relatively short and to take enough data-sets to create a phase light curve is then not that difficult task. P_{orb} of the system reveals how big the CV systems are. The most of the CVs with typical periods in range hours can fit inside Earth - Moon orbit.

Inspecting the Riter & Kolb catalogue Ritter & Kolb (2003) within the orbital period range from 1 hour to 1 day *(without the AM CVn systems)* it is found that almost half of all CVs in catalogue are the dwarf novae.

- 166 DNs 63% have $P_{orb} < 2h$
- 26 DNs 10% are found in the 2-3 h gap
- 70 DNs 27% are behind the gap with $P_{orb} > 3h$

The conventional idea about where the gap comes from points to internal structure changing in the secondaries. In some point of secondary star evolution it has a radius *(corresponds to its mass)* in excess of the equilibrium value. This force secondary to detaches from Roche lobe foe a while. The stellar wind is also very low during this period which cause disappearance of accretion disk. The period gap and the orbital period distribution per all the CVs and between the different CVs types is well shown on fig.3.2.

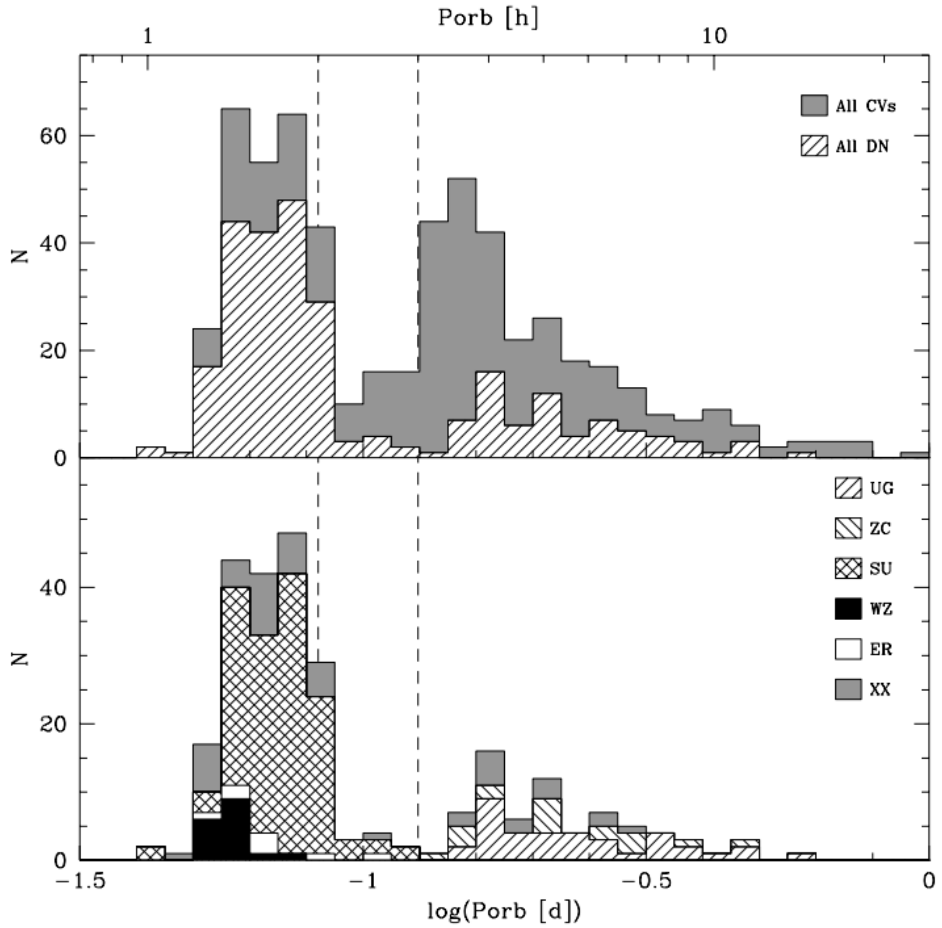

Figure 3.2: *Top panel*: the orbital period distribution of known CVs and dwarf novae from are shown in gray and shade Ritter & Kolb (2003). *Bottom panel*: the period distribution of known dwarf novae according to their subtypes, U Gem (UG), Z Cam (ZC), SU UMa (SU), WZ Sge (WZ), ER UMa (ER), and unclassified subtype (XX). The dashed lines represent the conventional 2-3h period gap Aungwerojwit (2007).

3.2 Magnetic cataclysmic variables

Magnetic CVs are these where the strong magnetic field significantly affects the accretion process. These systems are divided according to strength of their magnetic field to two categories:

- Polars, also called AM Herculis stars, $B_{wd} \sim 10^7 - 10^9 G$
- Intermediate polars $B_{wd} \sim 10^6 - 10^7 G$

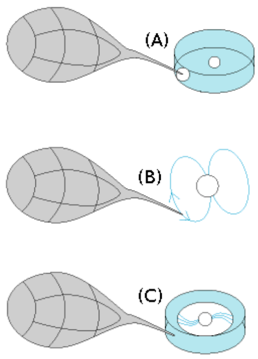

Figure 3.3: An illustration of difference between non-magnetic and magnetic CVs. *(A)* is an illustration of non-magnetic disk-type system, same as artist impression fig.3.1. *(B)* is a system with strongly magnetized WD called Polar where magnetic field prevent creations of accretion disk and the in-falling material forms an accretion stream following the magnetic field lines of WD. *(C)* is intermediate case between *(A)* and *(B)*, the not such strongly magnetized WD as one in polars destroying only inner part of accretion disk by his B_{wd} creating accretion curtain following its magnetic field lines.

3.2.1 Polars

The *(B)* part of fig.3.3 is how schematically polars looks like. The material from secondary is falling via the inner Lagrangian point towards to the primary, which is the highly magnetized WD as was mention before. The gas in the stream is ionized by collisions and X-rays from the accretion region on the WD. In some point at the stream's trajectory the magnetic energy density of the WD's field is sufficient to divert the stream from its free fall trajectory and force it to follow the magnetic field lines. Accretion therefore occurs over a small area near both or one of the magnetic poles of the WD. The magnetic field is assumed to be bipolar Cropper (1990).

How material traveling at roughly the escape velocity of the WD it approaches to the surface of the WD a very strong shock region is formed in accretion flow. The hard X-rays are emitted from post-shock region. Fraction of X-rays is reprocessed by the surface of WD and re-emitted as the softer X-rays component.

Free electrons close to the shock spiral around the magnetic field lines, therefore, emit strongly polarized cyclotron radiation. The magnetic field of WD is such strength that the cyclotron radiation is emitted in optical and near infra-red wavelengths.

In polars, the WD magnetic field is sufficiently strong to force the primary to rotate synchronously. The magnetic field therefore always present the same section to the incoming accretion stream. This is the principal distinguishing feature for polars (intermediate polars rotates asynchronous).

The principal defining characteristic of the polar CVs class is their strongly and variably circularly and linearly polarized optical emission. They are also characterized by high ratio of soft-to-hard X-ray luminosity and high excitation optical spectra with prominent He II 468.6 emission lines. For a review of the polars, see Cropper (1990) or Warner (1995).

3.2.2 Intermediate polars

The *(C)* part of fig.3.3 illustrates how can be intermediate polars imagined. They are CVs with not as strong magnetized WDs as in polars. This is causing a several important differences between polars and IPs. In IPs the other part of accretion disk exists, but at some distance of WD the kinetic energy density ρv^2 of gas in accretion disk is locally exceeded by the magnetic energy density $\frac{B^2}{8\pi}$ and within this radius the in-falling gas will be guided along magnetic field lines to accrete radially onto the WD creating kind of accretion curtain. For the spherical accretion is easy to calculate transition radius, because v is simply the free-fall velocity $\left(\frac{2GM}{r}\right)^{\frac{1}{2}}$, the radius is according Patterson (1994):

$$R_A = 3.7 \times 10^9 cm \dot{M}_{17}^{-\frac{2}{7}} M_{wd}^{-\frac{1}{7}} \mu_{32}^{\frac{4}{7}}, \tag{3.1}$$

where R_A is the *Alfven radius*, $\dot{M}_{17}$ is the accretion rate in units of $10^{17} g.s^{-1}$, M_{wd} is the mass of WD in units $M_\odot$ and μ_{32} is the magnetic moment of the WD in units of $10^{32} G.cm^3$. For disk accretion, the magnetospheric radius should be slightly smaller, theoretical estimates suggest $R_{mag} \approx 0.5 R_A$ Patterson (1994).

As the gas almost freely fals onto WD channeled along magnetic field lines, in some distance near the WD surface a stationary shock stands to convert the kinetic energy of the gas into thermal energy, Yuasa et al. (2010). The temperature of such shock heated gas is typically over 10keV and the density is low. The hard X-rays are emitted via optically thin thermal emission. Then the heated gas forms a post shock region *(PSR)* with a temperature gradient. The gas descends while it is cooled via X-ray emission and finally hits the surface of WD with small energy by emitting UV light Aizu (1973). This property makes from IPs very good targets for hard X-ray space missions. The closer look to PSR will be taken in the next chapter.

CHAPTER 4

Masses of white dwarfs in intermediate polars

As it was mentioned before, the mass of a WD is the most fundamental parameter in CVs. It is also the main parameter characterizing the accretion flow, the emission from the accretion region and, most importantly, it is the parameter which governs the dynamics of orbital motion of the system. The knowledge of WDs' masses in CVs plays a fundamental role in understanding the binary evolution.

Previous attempts to determine the WDs' masses in IPs using X-ray measurements did not succeed, because the data from different instruments led to different mass estimates. In all cases, the masses determined by the X-ray measurements where substantially higher than masses derived from the optical observations. The most notable example is XY Ari, which is an eclipsing IP with a very small uncertainty in the inclination (Ramsay et al. (1998)).

- RXTE spectrum yields 1.22 $M_\odot$
- ASCA data yields 1.27 – 1.4 $M_\odot$
- Ginga results 1.3 $M_\odot$
- the optical methods yields 0.78 – 1.03 $M_\odot$

Observations in hard X-rays over 20 KeV are crucial as they provide a clean signal, not contaminated by other system components such as the accretion disc or the main-sequence star and they avoid complications due to cold or warm absorbents as well as the fluorescence emission (Brunschweiger et al. (2009)). However, this method is not suitable because of the weakness of the X-ray flux. In spite of the fact that the IPs are among the brighter sources in the hard X-ray sky, their photon count is relatively low. Thus a sensitive instrument must be used for this kind of observations. At present, there are three instruments which are widely used for such observations: Swift/NASA Burst Alert Telescope, Hard X-ray Detector (HXD) onboard Suzaku/JAXA space mission and IBIS on-board INTEGRAL/ESA.

The idea how to study the post-shock region, the X-ray emission from IPs and then determine the mass of WD is to try to cover broad bands from soft to hard X-rays. Ideally, from 1keV up to 100 keV. In the softer X-rays below 10 keV there are, however, several other features present, but the photon flux in this band is much higher than in bands over 15 keV.

In this case, it is necessary to combine two different detectors, one for soft and one for hard X-rays. The optimal combination would be XMM-Newton for soft X-ray in range 1–10 keV and INTEGRAL for hard X-ray from 20–100 keV.

This combination provides a good compromise. The photon flux in the soft X-ray is high enough to allow short pointings of XMM with a good s/n ratio. However, the fitting model for such spectrum can be complicated because of the presence of several other features e.g. reflections or the 6.4 keV emission line.

The hard X-rays are important for the localization of the spectral energy cutoff so a good fit of the model, either power-law or bremsstrahlung, can be applied. INTEGRAL/IBIS is, due to a relatively good sensitivity and large field of view (FOV), a suitable instrument for observations in this band. The large FOV allows a good coverage of the X-ray sky enabling long exposures covering multiple objects in this band.

4.1 Post shock region

Reason why IPs are the most suitable for measurements of the mass of their WD companion then others CVs is their magnetic field, which is not as low as in non-magnetic CVs $B < 10^6$ but still weaker then in polars $B \gtrsim 10^7$. As was mentioned before, in IPs is the accretion disk destroyed in some distance from WD and accretion continues through accretion curtain, where the gas follows magnetic force lines. The resulting configuration is often know as an accretion column. From theory of spherical accretion (Frank et al. (2002)) we expect that accreting matter to be highly supersonic and therefore in free-fall above the WD's pole-caps.

The in-falling matter must be somehow decelerated to subsonic velocities in order to accrete, therefore we expect strong shock-wave in matter stream where the kinetic energy of infall

$$\frac{1}{2}\upsilon_{ff}^2 = GM_{wd}/R_{wd}, \tag{4.1}$$

will be turned into thermal energy. Because that $m_p \gg m_e$ the ions are these who brings the most of this kinetic energy supply. The kinetic energy of ions must by emitted, absorbed or re-emitted by WD. The luminosity corresponding to the typical accretion rate $\dot{M} \gtrsim 10^{16}\mathrm{g\,s^{-1}}$ will be of order $10^{33}\mathrm{erg\,s^{-1}}$ which greatly exceed any intrinsic luminosity (typically $\ll 10^{31}\mathrm{erg\,s^{-1}}$) that the WD may have as a result of left-over thermal energy in its degenerated core (Frank et al. (2002)).

The accretion luminosity is according to Frank et al. (2002):

$$L_{acc} \lesssim 2 \times 10^{29} f_{-2} m_1^{18/7} R^{-1/7} \, \mathrm{erg\,s^{-1}}, \tag{4.2}$$

where $f_{-2} = 10^2 f$ and f is a surface fraction.Which is much lower then the bolometric luminosities of observed CVs. Therefore, we must conclude that the infaling matter goes through strong shock which slows it down before reaching the WD surface.

Now we know that the shock gas is hot with characteristic (shock) temperature

$$T_s = \frac{3}{8}\frac{GM\mu m_H}{kR_{wd}} = 3.7 \times 10^8 m_1 R^{-1} \mathrm{K}. \tag{4.3}$$

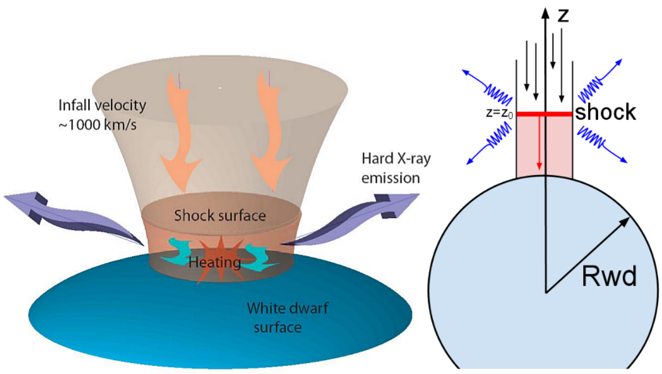

Figure 4.1: PSR, Krivonos Krivonos & Revnivtsev (2011)

4.1.1 Bremsstrahlung

Bremsstrahlung is a German word for breaking radiations, which is a radiations due to the acceleration of a charge in the Coulomb field of another charge also called as free-free emission. A full understanding of this process requires a quantum treatment, since photons of energies comparable to that of the emitting particle can be produced, Rybicki & Lightman (1979).

The electrostatic accelerations of the in its rest frame, parallel $a_{\|}$ and perpendicular $a_{\perp}$ to its direction of motion are:

$$\begin{aligned} a_{\|} = \dot{\upsilon}_x &= -\frac{eE_x}{m_e} \frac{\gamma {Z_e}^2 \upsilon t}{4\pi\varepsilon_0 m_e \left[b^2 + (\gamma\upsilon t)^2\right]^{2/3}}, \\ a_{\perp} = \dot{\upsilon}_z &= -\frac{eE_z}{m_e} \frac{\gamma {Z_e}^2 b}{4\pi\varepsilon_0 m_e \left[b^2 + (\gamma\upsilon t)^2\right]^{2/3}}, \end{aligned} \tag{4.4}$$

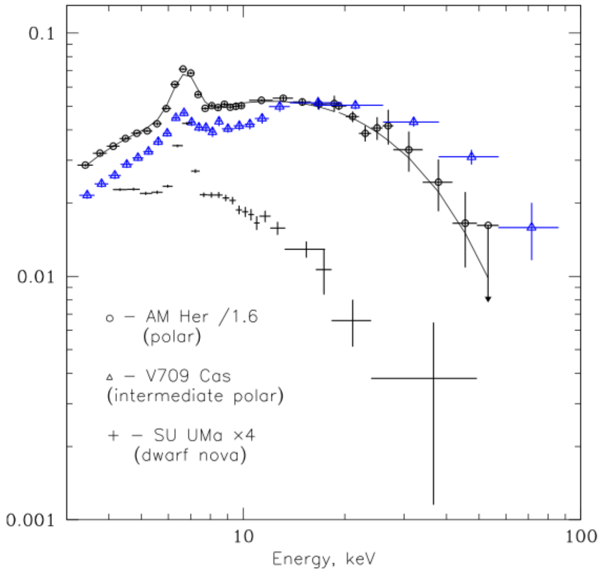

Figure 4.2: Typical broadband spectra of different CVs' classes, indicating that INTEGRAL observations in the hard X-ray energy band (17–60 keV) are biased toward detecting the hardest CVs – intermediate polars, Revnivtsev et al. (2008).

where Z_e is the charge of the nucleus, Longair (2011). Then we can take the Fourier transformation of the acceleration equations Eq.(4.4):

$$\begin{aligned} \dot{\upsilon}_x(\omega) &= \frac{1}{(2\pi)^{1/2}} \int_{-\infty}^{\infty} \frac{\gamma Z e^2 \upsilon t}{4\pi\varepsilon_0 m_e \left[b^2 + (\gamma \upsilon t)^2\right]^{2/3}} \exp(\mathrm{i}\omega t)\,\mathrm{d}t, \\ \dot{\upsilon}_z(\omega) &= \frac{1}{(2\pi)^{1/2}} \int_{-\infty}^{\infty} \frac{\gamma Z e^2 b}{4\pi\varepsilon_0 m_e \left[b^2 + (\gamma \upsilon t)^2\right]^{2/3}} \exp(\mathrm{i}\omega t)\,\mathrm{d}t. \end{aligned} \tag{4.5}$$

Changing variables to $x = \gamma \upsilon t / b$ will leads to:

$$\begin{aligned} \dot{\upsilon}_x(\omega) &= \frac{1}{(2\pi)^{1/2}} \frac{Z e^2}{4\pi\varepsilon_0 m_e} \frac{1}{\gamma b \upsilon} I_1(y), \\ \dot{\upsilon}_z(\omega) &= \frac{1}{(2\pi)^{1/2}} \frac{Z e^2}{4\pi\varepsilon_0 m_e} \frac{1}{b \upsilon} I_2(y), \end{aligned} \tag{4.6}$$

where $y = \omega b / \gamma \upsilon$. The integrals $I_1(y)$ and $I_2(y)$ are

$$I_1(y) = 2\mathrm{i}yK_0(y), \qquad I_2(y) = 2yK_1(y) \tag{4.7}$$

where K_0 and K_1 are modified Bessel functions of order zero and one, Longair (2011). The radiation spectrum of the electron encountering a charged nucleus therefore looks like:

$$\begin{aligned} I(\omega) &= \frac{e^2}{3\pi\varepsilon_0 c^3}\left[\left|a_{\parallel}(\omega)\right|^2 + |a_{\perp}(\omega)|^2\right] \\ &= \frac{Z^2 e^6}{24\pi^4\varepsilon_0^3 c^3 m_e^2 v^2}\frac{\omega^2}{\gamma 2\upsilon^2}\left[\frac{1}{\gamma^2}K_0^2\left(\frac{\omega b}{\gamma\upsilon}\right) + K_1^2\left(\frac{\omega b}{\gamma\upsilon}\right)\right] \end{aligned} \tag{4.8}$$

where b is the collision parameter.

The radiation spectrum showing both parallel and perpendicular accelerations to the motion direction of the electron is shown in fig.4.3. The perpendicular impulse has higher contribution, even in non-relativistic case, where $\gamma = 1$. In addition, this component cause significant radiation at low frequencies.

It is very useful to examine the behavior of the asymptotic limits of $K_0(y)$ and $K_1(y)$:

$$\begin{aligned} &y \ll 1 \qquad K_0(y) = -\ln y \qquad K_1(y) = 1/y, \\ &y \gg 1 \qquad K_0(y) = K_1(y) = (\pi/2y)^{1/2}\exp(-y). \end{aligned} \tag{4.9}$$

There is an exponential cut-off in high frequencies radiation spectrum

$$I(\omega) = \frac{Z^2 e^6}{48\pi^3\varepsilon_0^3 c^3 m_e^2 \upsilon^2}\frac{\omega}{\gamma\upsilon b}\left[\frac{1}{\gamma^2+1}\right]\exp\left(-\frac{2\omega b}{\gamma\upsilon}\right), \tag{4.10}$$

because of the duration of the relativistic collision, which is roughtly $\tau = 2b/\gamma\upsilon$. According to this, the dominant Fourier corresponds to $\upsilon \approx 1/\tau = \gamma\upsilon/2b$ and therefore to $\omega \approx \pi\upsilon\gamma/b$. Because $\omega \approx \gamma\upsilon/b$ there is only a little power emitted at grater frequencies then ω.

The low frequency spectrum has the form:

$$I(\omega) = \frac{Z^2 e^6}{24\pi^4\varepsilon_0^3 c^3 m_e^2 \upsilon^2}\frac{1}{b^2}\left[1 + \frac{1}{\gamma^2}\left(\frac{\omega b}{\gamma\upsilon}\right)^2 \ln^2\left(\frac{\omega b}{\gamma\upsilon}\right)\right], \tag{4.11}$$

In the limit case $\omega b/\gamma\upsilon \ll 1$, the second term in square brackets of Eq.(4.11) is negligible and hence the good approximation for low frequency intensity spectrum is

$$I(\omega) = \frac{Z^2 e^6}{24\pi^4\varepsilon_0^3 c^3 m_e^2 \upsilon^2} = K. \tag{4.12}$$

We could guessed that the low frequency bremsstrahlung spectrum would be flat if we consider that the momentum impulse is a delta function, thus the collision duration is much less then the waves period. The Fourier transform of a delta function is the flat spectrum $I(\omega) = $ constant. The spectrum will be flat approximation up to the frequency $\omega = \gamma\upsilon/b$, above this, it will falls of exponentially. Note also that γ disappeared from Eq.(4.12), even in the relativistic case. This means that the momentum impulse is the same in the relativistic and non-relativistic cases, for detailed derivation see Longair (2011), Jackson (1999).

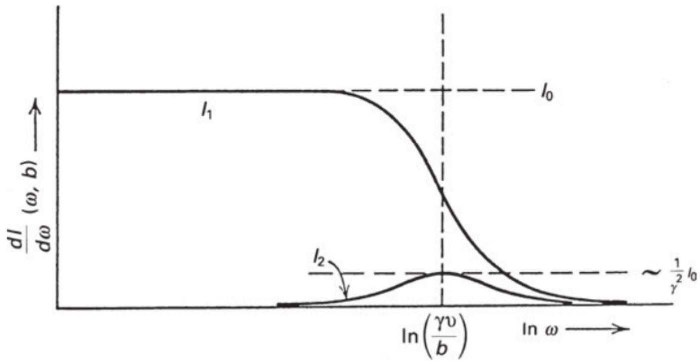

Figure 4.3: The bremsstrahlung spectrum from the acceleration of the electron parallel and perpendicular to its initial direction of motion as was displayed in Jackson (1999), or Rybicki & Lightman (1979).

Now we can integrate over all the collision parameters which contribute to the radiation at frequency ω:

$$I(\omega') = \int_{b'_{min}}^{b'_{max}} 2\pi b' \gamma N \upsilon K \mathrm{d}b' = \frac{Z^6 e^6 \gamma N}{12\pi^3 \varepsilon_0^3 c^3 m_e^2} \frac{1}{\upsilon} \ln\left(\frac{b'_{max}}{b'_{min}}\right), \tag{4.13}$$

note that if the electron is moving by relativistic speed, because of the relativistic length contractions, it observed more nuclei enhanced by a factor γ. $N' = \gamma N$, where N is nuclear density .

4.1.2 Thermal bremsstrahlung

In previous sub-section we derive the breaking radiation spectrum for one electron, but in real plasma at temperature T is necessary to integrate single partition spectrum over the collision parameters and over the Maxwell distribution of electron velocities

$$N_e(\upsilon)\mathrm{d}\upsilon = 4\pi N_e \left(\frac{m_e}{2\pi kT}\right)^{2/3} \upsilon^2 \exp\left(-\frac{m_e \upsilon^2}{2kT}\right) \mathrm{d}\upsilon. \tag{4.14}$$

The approximate expression for the spectral emissivity of a plasma of electron density N_e in the low frequency limit is

$$I(\omega) \approx \frac{Z^2 e^6 N N_e}{12\sqrt{3}\pi^3 \varepsilon_0^3 c^3 m_e^2} \left(\frac{m_e}{kT}\right)^{1/2} g(\omega, T), \tag{4.15}$$

where $g(\omega, T)$ is known as Gaunt factor. It is important to realize that the low frequency thermal bremsstrahlung spectrum is almost independent of frequency, the only dependence upon ω comes from the slightly varying function in the Gaunt factor.

At the high frequencies the spectrum of thermal bremsstrahlung exponentially cuts off according to $\exp(-\hbar\omega/kT)$. This behavior is reflecting the exponential decrease in the electrons population in hard energy tail of Maxwell distribution.

Finally, we can get the total energy loss by the plasma by integrating the spectral emissivity over all possible frequencies, because of the exponential cut-off, the integration should be helds from 0 to $\omega = kT/\hbar$ which leads to

$$-\frac{\mathrm{d}E}{\mathrm{d}t} = (\text{constant})\, Z^2 T^{1/2} \bar{g} N N_e. \tag{4.16}$$

Detailed calculations give the following results, int terms of frequency υ rather then the angular frequency ω. The spectral plasma emissivity according to Longair (2011) is

$$\begin{aligned} K_\upsilon &= \frac{1}{3\pi^2}\left(\frac{\pi}{6}\right)^{1/2} \frac{Z^2 e^6}{\varepsilon_0^3 c^3 m_e^2}\left(\frac{m_e}{kT}\right)^{1/2} g(\upsilon, T) N N_e \exp\left(-\frac{h\upsilon}{kT}\right), \\ &= 6.8\times 10^{-51} Z^2 T^{-1/2} N N_e g(\upsilon, T) \exp\left(-\frac{h\upsilon}{kT}\right) \mathrm{W\,m^{-3}\,Hz^{-1}}, \end{aligned} \tag{4.17}$$

where both: densities of electrons N_e and of nuclei N are in barticles per m^3. At frequencies $h\upsilon \ll kT$, the Gaunt factor has only a logarithmic dependence on the frequency. Therefore for radio and X-ray wavelengths are suitable following forms:

$$\begin{aligned} \mathrm{Radio}: g(\upsilon, T) &= \frac{\sqrt{3}}{2\pi}\left[\ln\left(\frac{128\varepsilon_0^2 k^3 T^3}{m_e e^4 \upsilon^2 Z^2}\right) - \gamma^{1/2}\right], \\ \mathrm{X-ray}: g(\upsilon, T) &= \frac{\sqrt{3}}{2\pi}\ln\left(\frac{kT}{h\upsilon}\right), \end{aligned} \tag{4.18}$$

where $\gamma = 0.577$ is the Euler's constant.

The total loss rate of the plasma is

$$-\left(\frac{\mathrm{d}E}{\mathrm{d}t}\right)_{brems} = 1.435\times 10^{-40} Z^2 T^{1/2} \bar{g} N N_e \,\mathrm{W\,m^{-3}}. \tag{4.19}$$

Detailed calculation show that the average value of the Gaunt factor $\bar{g}$ lies in the range $1.1-1.5$, then $\bar{g} = 1.2$ will be a good approximation (Longair (2011)). To apply a suitable Gaunt factors in the thermal bremsstrahlung formula is nontrivial and complex task. Several useful papers about suitable Gaunt factors were published. One of the more recent is that from Sutherland (1998).

4.2 WD mass estimations methods

CHAPTER 5

Data analysis

5.1 INTEGRAL

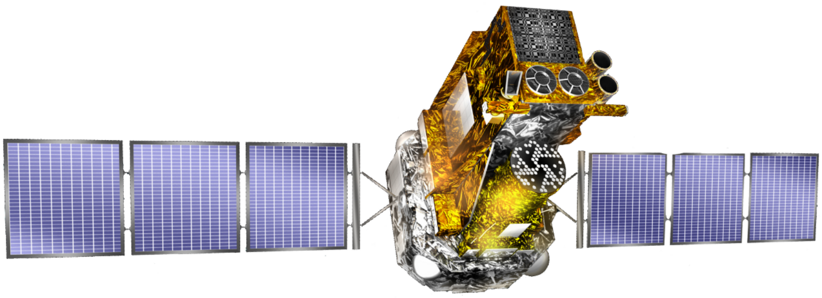

Figure 5.1: INTEGRAL

5.2 XMM-Newton

5.3 Results

5.4 Discussion

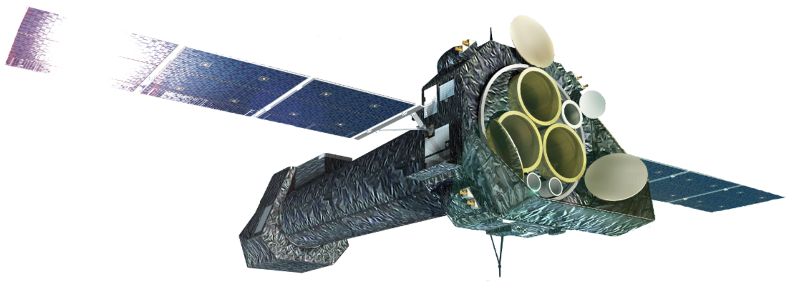

Figure 5.2: XMM-Newton

CHAPTER 6

Conclusions

Bibliography

Adams, D. 1979, The Hitchhiker's Guide to the Galaxy (Great publishing house of Ursa Minor Beta)

Aizu, K. 1973, Progress of Theoretical Physics, 49, 1184

Arnaud, Smith, S. 2011, Handbook of X-ray Astronomy (Cambridge University Press)

Aungwerojwit, A. 2007, PhD Thesis

Brunschweiger, J., Greiner, J., Ajello, M., & Osborne, J. 2009, A&A, 496, 121

Butters, O. W., Norton, A. J., Mukai, K., & Tomsick, J. A. 2011, A&A, 526, A77

Camenzind, M. 2007, Compact Objects in Astrophysics (Springer)

Carroll, B. W. & Ostlie, D. A. 2007, An Introduction to Modern Astrophysics, second edition (Pearson Inc.)

Chandrasekhar, S. 1939, MNRAS, 99, 673

Cropper, M. 1990, Space Science Reviews, 54, 195

Forman, W., Jones, C., Cominsky, L., Julien, P., Murray, S., Peters, G., Tananbaum, H., & Giacconi, R. 1978, ApJS, 38, 357

Frank, J., King, A., & Raine, D. 2002, Accreation Power in Astrophysics Third Edition (University Press, Cambridge)

Hamada, T. & Salpeter, E. E. 1961, ApJ, 134, 683

Jackson, J. D. 1999, Classical Electrodynamics (New York: John Wiley)

Kitchin, C. R. 2009, Astrophysical Techniques fifth edition (Taylor & Francis Group)

Kleczek, J. 1957, Interior of Stars (Press of Czechoslovak Academy of Science)

Krivonos, R. & Revnivtsev, M. 2011, Galactic Difuse Emission slides from presentation (The Extreme and Variable High Energy Sky, Workshop)

Krivonos, R., Revnivtsev, M., Churazov, E., Sazonov, S., Grebenev, S., & Sunyaev, R. 2007, A&A, 463, 957

Landi, R., Bassani, L., Dean, A. J., Bird, A. J., Fiocchi, M., Bazzano, A., Nousek, J. A., & Osborne, J. P. 2009, MNRAS, 392, 630

Longair. 2011, High Energy Astrophysics Third Edition (University Press, Cambridge)

Middleton, M. J., Cackett, E. M., Shaw, C., Ramsay, G., Roberts, T. P., & Wheatley, P. J. 2012, MNRAS, 419, 336

Mirabel, I. F. 2002, ASP Conference Series

Nauenberg, M. 1972, ApJ, 175, 417

Padmanabhan, T. 2001, Theoreticl Astrophysics Volume II: Stars and Stellar Systems (Cambridge University Press)

Patterson, J. 1994, Publications of the Astronomical Society of the Pacific, 106, 209

Ramsay, G., Cropper, M., Hellier, C., & Wu, K. 1998, MNRAS, 297, 1269

Revnivtsev, M., Sazonov, S., Krivonos, R., Ritter, H., & Sunyaev, R. 2008, A&A, 489, 1121

Ritter, H. & Kolb, U. 2003, A&A, 404, 301

Rothschild, R. E., Gruber, D. E., Knight, F. K., Matteson, J. L., Nolan, P. L., Swank, J. H., Holt, S. S., Serlemitsos, P. J., Mason, K. O., & Tuohy, I. R. 1981, ApJ, 250, 723

Rybicki, G. B. & Lightman, A. P. 1979, Radiative Processes in Astrophysics (John Wiley & Sons, Inc.)

Sazonov, S., Revnivtsev, M., Gilfanov, M., Churazov, E., & Sunyaev, R. 2006, A&A, 450, 117

Shapiro, S. L. & Teukolsky, S. A. 2004, Black holes, white dwarfs, and neutron stars: The physics of compact objects, ed. Shapiro, S. L. & Teukolsky, S. A.

Suh, I.-S. & Mathews, G. J. 2000, ApJ, 530, 949

Suleimanov, V., Revnivtsev, M., & Ritter, H. 2005, A&A, 435, 191

Sutherland, R. S. 1998, MNRAS, 300, 321

Warner, B. 1995, Cataclysmic Variable Stars (University Press, Cambridge)

Yuasa, T., Nakazawa, K., Makishima, K., Saitou, K., Ishida, M., Ebisawa, K., Mori, H., & Yamada, S. 2010, A&A, 520, A25+

Appendix

this will be the appendix

Table 1: Estimated WD masses from previous reports ...

System	Suzaku XIS+HXD M_{WD}	Swift BAT M_{WD}	RXTE PCA+HEXTE M_{WD}	RXTE PCA M_{WD}	Ginga LAC M_{WD}	ASCA SIS M_{WD}	This work XMM & Integral M_{WD}
FO Aqr							
XY Ari							
MU Cam							
BG CMi							
V709 Cas							
TV Col							
TX Col							
YY Dra							
PQ Gem							
EX Hya							
NY Lup							
V2400 Oph							
AO Psc							
V1223 Sgr							
RX J2133							
IGR J17303							